Analysis of small angle neutron scattering from nanocrystalline niobium carbide powders using global scattering functions

G. D. BOKUCHAVA*, Yu. E. GORSHKOVA
Frank Laboratory of Neutron Physics, Joint Institute for Nuclear Research, 141980 Dubna, Russia

Small angle neutron scattering (SANS) from nanocrystalline niobium carbide powders was analyzed using global scattering functions. The samples were prepared by high-energy ball milling technique with different milling durations. The experimental data analysis has shown that SANS spectra from such material can be described in terms of combined scattering from surface fractal aggregates and nanocrystalline subparticles with a diffusive surface. Within the applied model the degree of particle polydispersity, nanoparticles size and their distribution versus milling duration were analyzed.

(Received May 7, 2015; accepted June 24, 2015)

Keywords: Small angle neutron scattering, Microstructure, Nanomaterials

1. Introduction

Nowadays nanomaterials are coming into use in electronics, optics, industry, healthcare, cosmetics and many other areas. Nanomaterials can be metals, alloys, intermetallides, ceramics, polymers, semiconductors, composites, etc. Usually they contain nanoparticles, smaller than 100 nm in at least one dimension. Materials with structure at the nanoscale often have unique mechanical, electrical, magnetic, optical, chemical and other properties that differ from those of bulk materials. Furthermore, nanomaterials are of great scientific interest since at the nanoscale they often demonstrate size-dependent physical and chemical properties while a bulk material with same chemical composition have constant physical properties regardless of its size. In most cases size-dependent properties of nanomaterials can be tuned via various synthesis techniques: plasmochemical, gas-phase and detonation-induced synthesis, vapour condensation, chemical deposition from colloidal solutions, pyrolysis, mechanical milling, severe plastic deformation, crystallization of amorphous alloys, etc. [1]. One of the most efficient methods for the preparation of sufficient amount of nanomaterial is high-energy ball milling technique, which allows obtaining nanoparticles with size of down to 2-4 nm. In addition, high-energy ball milling technique is often used to process new materials such as oxide dispersed strengthened (ODS) steels, nickel- and iron-based superalloys for applications in the power engineering and aerospace industry.

Various carbide materials are widely used in modern engineering industry to improve mechanical and chemical properties of structural alloy and tool steels and hard alloys for operation at high temperatures and extreme loads. For example, niobium alloyed steel acquires high corrosion resistance without losing its plasticity. Some niobium compounds (carbides, borides) are used in the production of most heat-resistant super-hard alloys to enhance their resistance to wear and microchipping during machining of steels. One of the most heat-resistant materials is niobium carbide with a melting point of ~3800 K. For this reason, niobium carbide alloyed with zirconium and uranium carbides is used as a most important structural material for nuclear fuel elements.

For the practical applications of these high technological materials, it is vital to control their physical and chemical properties, which are greatly dependent on the particle size. Small-angle scattering (SAS) is a widespread method for materials microstructure characterization at the nanometer length scale. Therefore, the aim of the present SANS investigation of a ball milled NbC powders was to analyze their microstructural characteristics, i.e. to know particle size and shape, and their distribution in such nanocrystalline materials.

2. Materials and methods

Four powder samples of nanocrystalline nonstoichiometric niobium carbide NbC_y ($y \approx 0.93$) were obtained by high-energy ball milling [2] of the initial coarse grain powder with different milling duration: T = 0, 1, 5, 15 hours. Initial single-phase powder was synthesized by high-temperature solid-phase vacuum sintering. The material has FCC cubic structure (a = 4.4658 Å) and rather high degree of homogeneity of the original composition ($\Delta y \approx 0.01$).

SANS experiments have been performed on the YuMO small-angle time-of-flight neutron diffractometer at the IBR-2 pulsed reactor in FLNP JINR (Dubna, Russia) [3]. Samples of niobium carbide powders were placed into a 1 mm thick quartz cuvette. All measurements were performed at room temperature. Two ring wire He^3-detectors [4] at distances of 4 m and 13 m from the sample position were used in our experiment. The scattered intensity (differential cross section per sample volume)

was registered as a function of the momentum transfer modulus $Q = (4\pi/\lambda)\sin(\theta/2)$, where θ is the scattering angle and λ is the incident neutron wavelength. An incident neutron beam distribution provides an available wavelength range of 0.5 ÷ 8 Å, which corresponds to momentum transfer range Q of 0.0068 ÷ 0.54 Å^{-1}. The measured SANS spectra were converted to the absolute scale by normalization to the incoherent scattering cross section of standard vanadium sample. Additionally the measured spectra were corrected taking into account scattering from the setup and empty cuvette, as well as the background.

3. Results and discussion

Experimental SANS curves in the double logarithmic scale from all studied samples are presented in Fig. 1. The measured SANS spectra demonstrate quite smooth patterns over the whole available Q-range which points to high polydispersity of the studied system. Some specific features (linear regions and inflection points) of the scattering curves can be easily distinguished in Porod-Debye plot of $I(Q)Q^4$ vs. Q^4 (Fig. 2).

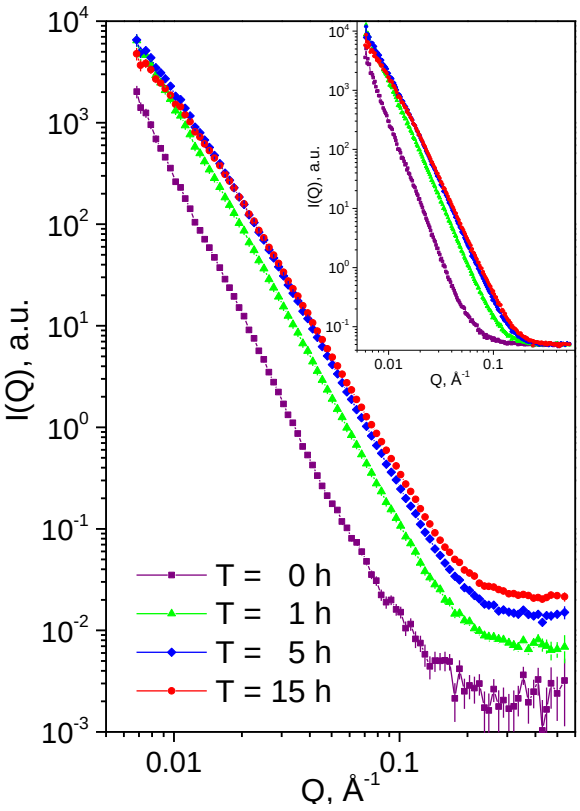

Fig. 1. Experimental SANS curves for series of NbC powders with different milling durations. The inset shows the same data with subtracted background constant C obtained from least square fit (see below).

Usually SAS curves are characterized by two main features: the Guinier region and the Porod region. Standard linear plots are applied within these regions to fit SAS data. Thus the Guinier linear plot gives a value of a gyration radius that characterizes the size of the scattering particles, while the Porod plot gives an exponent value which characterizes a substructural dimensionality. Therefore, from estimated fractal dimension the particle shape can be determined. According to the Porod law, the exponent value equals to 4 for particles with smooth sharp interface. The power-law exponent in the range between 1 and 3 corresponds to mass fractals [5], exponents between 3 and 4 indicate surface fractals [6], and between 4 and 6 – diffuse surface [7].

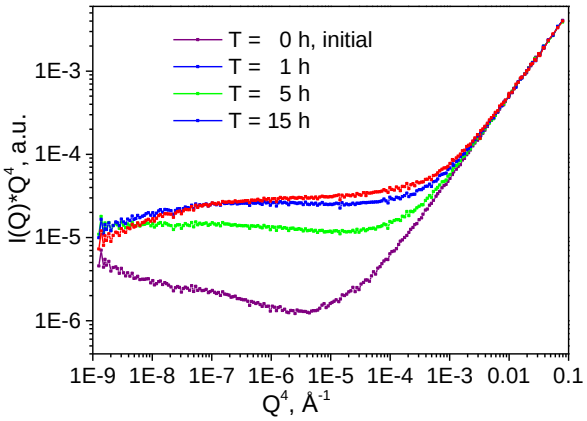

Fig. 2. Experimental SANS curves plotted as $I(Q)Q^4$ vs. Q^4 with subtracted background for series of NbC powders with different milling durations.

The observed pattern for the niobium carbide is typical for scattering from two-level hierarchical structure with a different characteristic length scale and aggregation type for each level. At that first structural level corresponds to scattering from aggregates with surface fractal structure (small Q-values) while the second one - to scattering from compact non-aggregated subparticles (high Q-values).

Measured SANS curves $I(Q)$ were analyzed using the model suggested by G. Beaucage [8, 9] (Fig. 3). This model uses unified global scattering function over the whole available Q-range as a combination of exponential and power-law parts to fit the Guinier and Porod regions with a smooth transition region between them. Within this model, the observed scattering intensity was treated in the frame of the unified global scattering function for two structural levels:

$$I(Q) = G\exp\left(\frac{-Q^2R_g^2}{3}\right) + B\exp\left(\frac{-Q^2R_{gS}^2}{3}\right)\left(\frac{1}{Q^*}\right)^P + \\ + G_S\exp\left(\frac{-Q^2R_{gS}^2}{3}\right) + B_S\left(\frac{1}{Q_S^*}\right)^{Ps} + C, \quad (1)$$

where G and B are Guinier and Porod scale factors, correspondingly, depending on the particle number

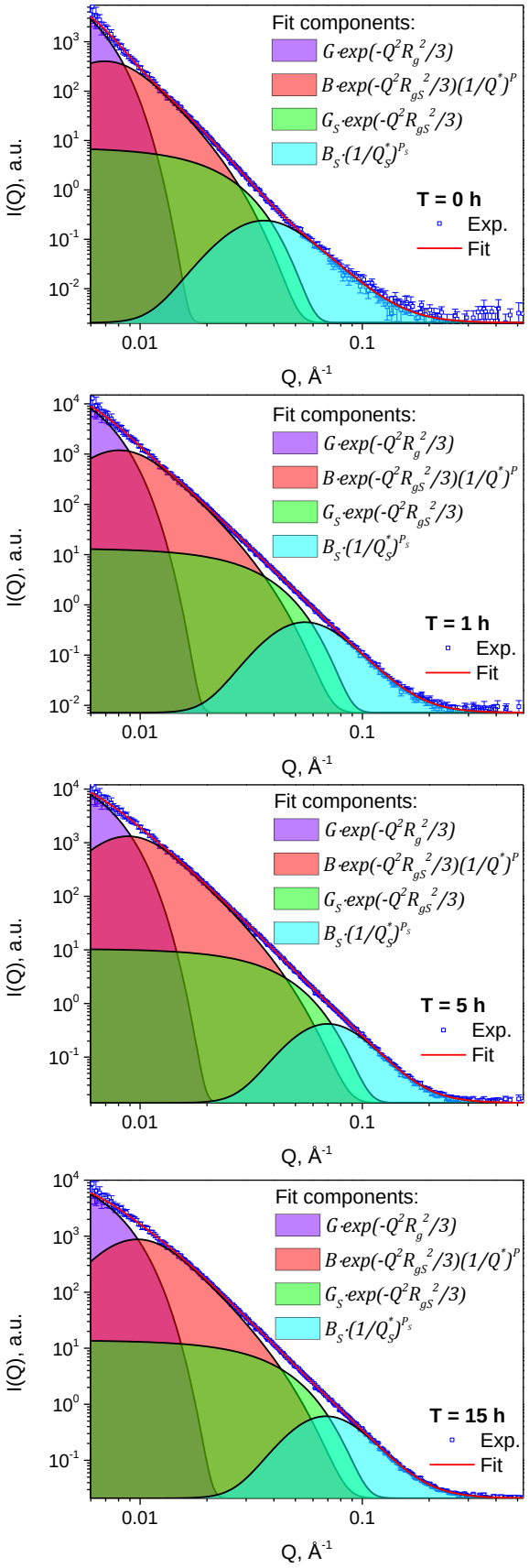

Fig. 3. Least square fits of experimental SANS curves. Experimental points, unified global scattering function for two structural levels and corresponding fit components according to Equation (1) are shown.

density and contrast, R_g is the radius of gyration, C is the residual incoherent background, P is the exponent of the power-law decrease. Variables Q and Q^* are renormalized in the power laws as follows:

$$Q^* = Q/\left[erf\left(\frac{kQR_g}{\sqrt{6}}\right)\right]^3 \text{ and } Q_S^* = Q/\left[erf\left(\frac{k_SQR_{gS}}{\sqrt{6}}\right)\right]^3,$$

where k and k_S are the empirical constants equal to 1.0 or 1.06. Parameters without index and with the index S correspond to the aggregates and to the subparticle scattering levels, respectively.

Microstructural parameters as a function of milling duration obtained from least square fit of experimental SANS curves for series of NbC powders are presented in Figs. 4-8 and in the Table 1.

Table 1. Parameters of the least square fit of the experimental curves according to the Equation (1) and calculated corresponding parameters of the lognormal size distribution for subparticles.

T, h	R_g, Å	R_{gS}, Å	D, Å	D_S, Å	P
0	423.95(7)	83.28(5)	1094.63	215.04	3.71(3)
1	368.86(3)	54.55(2)	952.39	140.84	3.70(1)
5	337.93(3)	43.10(2)	872.53	111.28	3.57(1)
15	305.04(4)	43.83(3)	787.61	113.17	3.46(2)

T, h	P_S	β_S	PDI_{nS}	σ	R_{0S}, Å
0	4.02(3)	0.01(2)	4.72(4)	0.36(2)	43.94(5)
1	4.46(1)	0.23(1)	6.93(2)	0.37(1)	28.90(1)
5	4.57(1)	0.28(1)	8.72(2)	0.38(1)	21.56(1)
15	4.45(2)	0.22(1)	8.72(1)	0.39(1)	20.64(2)

It was found that gyration radii of aggregates and subparticles expectedly exhibits common tendency to decrease with increasing milling duration (Fig. 4). At the same time it is remarkable that gyration radius of aggregates R_g steadily decreases which can be interpreted as a permanent refinement of aggregates over the whole range of milling durations T. Meanwhile the gyration radius of nanocrystalline subparticles R_{gS} falls down sharply from initial state for short milling duration (1 hour) and then remains almost constant for longer milling durations (5 and 15 hours). If the spherical shape is assumed for aggregates and subparticles in monodisperse approximation their diameters can be estimated from radius of gyration as $D = 2(5/3)^{1/2}R_g$ (see Table 1).

A Guinier scale factor G exhibits regular decrease with milling duration increase reflecting the decrease of average particle volume. Meanwhile scaling factor G_S for subparticles demonstrates more irregular behavior (Fig. 5). At subparticles structural level both Porod scale factors B and B_S exhibit regular monotonous growth which can be attributed to increase of subparticles number and their surface area with increasing the milling duration (Fig. 6).

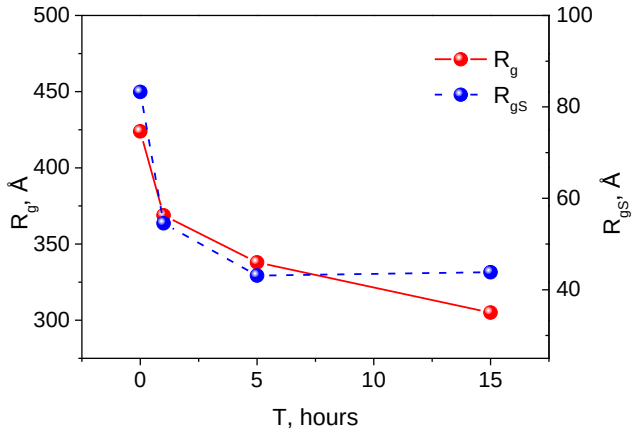

Fig. 4. The gyration radii of aggregates R_g and nanocrystalline subparticles R_{gS} vs. milling duration.

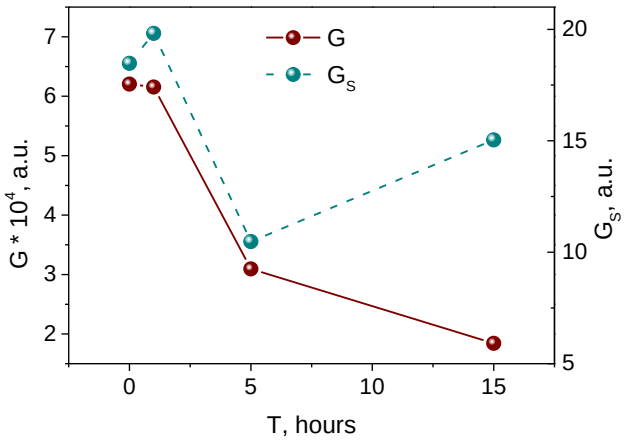

Fig. 5. Guinier scale factors G and G_S for aggregates and nanocrystalline subparticles structural levels.

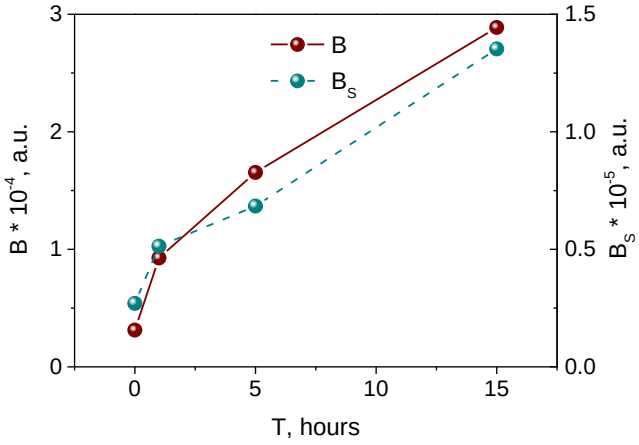

Fig. 6. Porod scale factors B and B_S for aggregates and nanocrystalline subparticles structural levels.

The residual incoherent background parameter *C* shows almost constant increase with increasing the milling duration (Fig. 7). It should be noted that the behavior of background parameter *C* correlates well with increase in Porod scale factors and corresponding decrease in radii of gyration. Therefore, the increase in residual incoherent background can be explained by gain in specific surface area of the system of milled particles, which leads to an increase in hydrogen absorption capacity of the studied material. In our case, the presence of some amount of hydrogen in the studied samples due to the adsorption of water from atmospheric air can be considered as the main source of incoherent background.

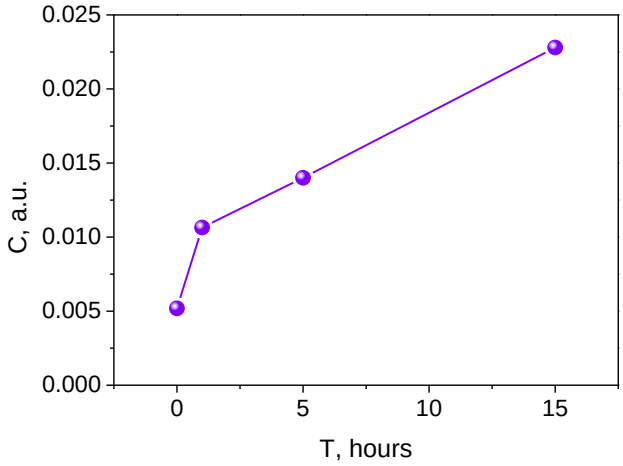

Fig. 7. Residual incoherent background parameter C vs. milling duration.

The analysis of deviation from the Porod power-law asymptotic behavior in small-angle scattering curve allows characterizing the fractal dimension of the system. Fractals are self-similar structures that exhibit a self-similar repeating pattern and appear identical at define range of length scales. Mass and surface fractals exhibit quite different behavior from the scattering viewpoint, hence from the Porod plot the nature of the scattering structure (i.e. particle shape) can be guessed.

The values of power-law exponents for first structural level obtained from non-linear least square fit procedure varies slightly within the range $P = 3.46 \div 3.71$ which corresponds to fractal-type organization of the clusters, i.e. aggregates with fractal surface structure (Fig. 8).

At the same time in the initial non-milled state of the material the second structural level (subparticles) exhibits a power-law type scattering in accordance with the Porod's law and with corresponding exponent value $P_S = 4.02(3)$. For this reason, the second structural level should be considered as subparticles with sharp interfaces in non-milled state of the material. In addition, for milled material the subparticles structural level demonstrates a power-law type scattering with the power-law exponent values within the range $P_S = 4.45 \div 4.57$ which is slightly higher than the value for particles with smooth sharp interface (equal to 4 according to Porod law). Such type of deviation from Porod law is characteristic feature for the particles with so-called diffusive interface.

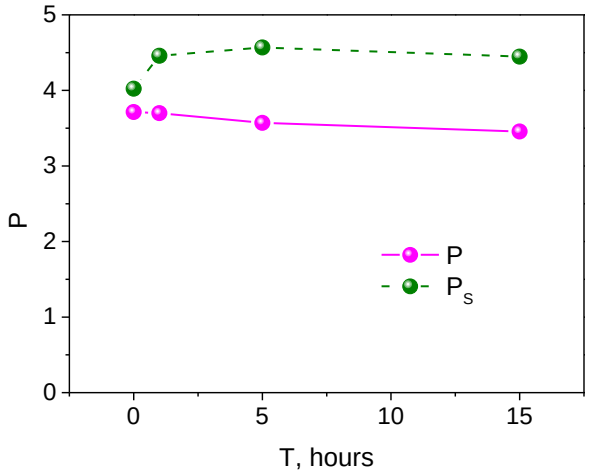

Fig. 8. The power-law exponent parameters P and P_s for aggregates and subparticles vs. milling duration.

The example of analysis of nanoparticle size distributions over wide range scattering vector Q from SANS curves was given in [10]. For this reason, a generalized index of polydispersity for symmetric particles with a sharp boundary was introduced as a dimensionless ratio:

$$PDI = BR_g^4/G. \quad (2)$$

Usually in practice, the spherically normalized value of polydispersity index is used:

$$PDI_n = BR_g^4/(1.62G), \quad (3)$$

where 1.62 is the value of PDI for homogeneous monodisperse spherical particles (the lowest possible value).

In [11, 12], it was shown that the similar approach may be used to analyze the polydispersity of particles with a diffusive surface. Here it is convenient to introduce the power-law exponent in the form $P_S = 4 + 2\beta$, where β is small parameter ($0 < \beta < 1$) describing the deviation from the Porod power-law in small-angle scattering. In this case, the polydispersity indices PDI and PDI_n are introduced as

$$PDI = BR_g^{4+2\beta}/G, \quad (4)$$
$$PDI_n = BR_g^{4+2\beta}/[t(\beta)G],$$

where $t(\beta)$ is renormalization parameter:

$$t(\beta) = \frac{1}{8}[(\beta+1)(\beta+2)(\beta+3)\Gamma(\beta+1)]^2 \times$$
$$\times \left[\frac{12}{(\beta+4)(\beta+5)}\right]^{2+\beta} \cong 1.62 + 1.78\beta + 0.88\beta^2.$$

For particle polydispersity analysis from small angle scattering data the approximation of the lognormal distribution of spherical particles is often used due to its simplicity:

$$f(R) = exp[-ln^2(R/R_0)/2\sigma^2]/[R\sigma\sqrt{2\pi}], \quad (5)$$

where R_0 is the most probable radius and σ is the mean squared deviation of the logarithm of the radius.

Furthermore, these two parameters can be derived from the experimental SANS data fit by unified global scattering function [see 10, 11] through normalized polydispersity index:

$$\sigma = \left[\frac{\ln(\mathrm{PDI_n})}{12 + 10\beta + 2\beta^2}\right]^{1/2}, \quad (6)$$

$$R_0 = R_g\left[\frac{(\beta+4)(\beta+5)}{12\exp(14\sigma^2)}\right]^{1/2}.$$

For studied material PDI_n index increases from 4.72 for initial material to 8.72 for milled samples (at milling durations of T = 5, 15 hours), exhibiting rather high polydispersity degree. Using these values of PDI_n index the parameters for the lognormal particle-size distribution (the most probable radius R_0 and the mean squared deviation of the logarithm of the radius σ) were calculated (Fig. 9) for all measured SANS curves.

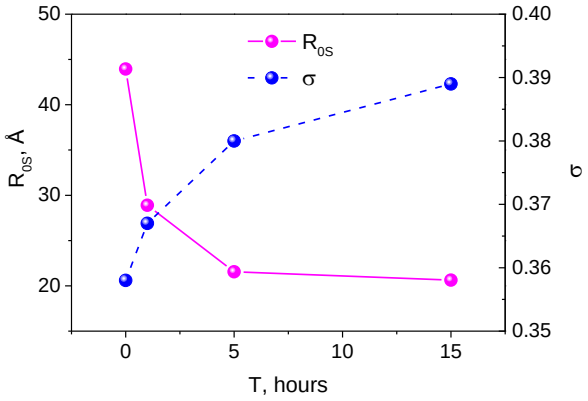

Fig. 9. Lognormal size distribution parameters the most probable radius R_0 and the mean squared deviation of the logarithm of the radius σ for nanocrystalline subparticles vs. milling duration.

Corresponding lognormal particle size distribution $f(R)$ varies significantly depending on the milling duration. As it can be seen from Fig. 10 the relatively broad size distribution for initial non-milled material distribution becomes less wide during the milling process, which is accompanied by a simultaneous decrease in the mean particle size. Numerical evaluations show that the particle size reduction makes the main contribution to this effect. While the contribution from changes of mean squared deviation σ is negligibly small, since it varies slightly in the range of 0.36 ÷ 0.39.

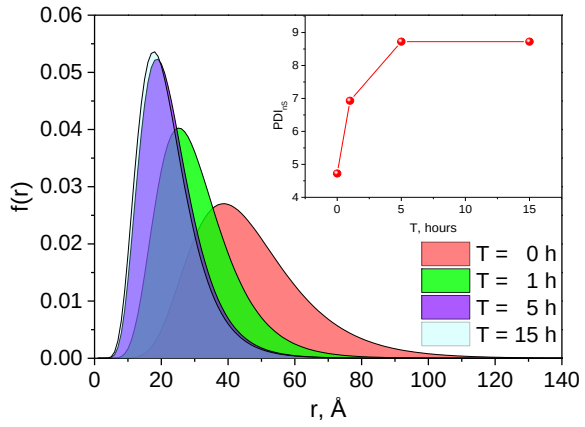

Fig. 10. Lognormal size distributions of nanocrystalline subparticles plotted for different milling durations. The inset shows normalized polydispersity index PDI_n dependence vs. milling duration.

4. Conclusions

The SANS results revealed that two hierarchical structural levels are clearly observed in the scattering data from ball milled nanocrystalline niobium carbide powders. First structural level corresponds to aggregates with fractal surface and it is characterized by its own gyration radius R_g in the range from 424 to 305 Å depending on milling duration. Second structural level corresponds to compact non-aggregated subparticles. The analysis of deviation from the Porod power-law asymptotic behavior in small-angle scattering curve allowed characterizing them as subparticles with diffusive interface. Estimated gyration radius R_{gS} of subparticles varies from 83 to 43 Å. Using normalized polydispersity index PDI_n lognormal distributions of subparticles sizes were calculated assuming their spherical shape. The obtained results demonstrate the power and utility of the SANS method in characterizing microstructure, particles size, and their distribution in these nanocrystalline materials.

Acknowledgements

This work was supported by the Russian Foundation for Basic Research and Moscow Region Government (project No. 14-42-03585_r_center_a). The authors thank D.V. Solovjov for experimental assistance. The authors are in debt to O.V. Tomchuk for useful discussions.

References

[1] A.A. Rempel, Russ. Chem. Rev. **76 (5)**, 435 (2007).
[2] A.I. Gusev, A.S. Kurlov, Inorganic Materials. **51**(1), 29 (2015).
[3] Y.M. Ostanevich, Macromol. Chem. Macromol. Symp. **15**, 91 (1988).
[4] A.I. Kuklin, A.Kh. Islamov, V.I. Gordeliy, Neutron News. **16(3)**, 16 (2005).
[5] J. Teixeira, J. Appl. Cryst. **21**, 781 (1988).
[6] P.W. Schmidt, J. Appl. Cryst. **24**, 414 (1991).
[7] P.W. Schmidt, D. Avnir, D. Levy, A. Hohr, M. Steiner, A. Roll, J. Chem. Phys. **94**, 1474 (1991).
[8] G. Beaucage, J. Appl. Cryst. **28**, 717 (1995).
[9] G. Beaucage, J. Appl. Cryst. **29**, 134 (1996).
[10] G. Beaucage, H.K. Kammler, S.E. Pratsinis, J. Appl. Cryst. **37**, 523 (2004).
[11] O.V. Tomchuk, L.A. Bulavin, V.L. Aksenov, V.M. Garamus, O.I. Ivankov, A.Ya. Vul', A.T. Dideikin, M.V. Avdeev, J. Appl. Cryst. **47**, 642 (2014).
[12] O.V. Tomchuk, D.S. Volkov, L.A. Bulavin, A.V. Rogachev, M.A. Proskurnin, M.V. Korobov, M.V. Avdeev, J. Phys. Chem. **119**, 794 (2015).

*Corresponding author: gizo@nf.jinr.ru